Nat. Hazards Earth Syst. Sci. Discuss., 3, 3077–3117, 2015
www.nat-hazards-earth-syst-sci-discuss.net/3/3077/2015/
doi:10.5194/nhessd-3-3077-2015

Natural Hazards and Earth System Sciences
Discussions
Open Access

Runup parameterization and beach vulnerability assessment on a barrier island: a downscaling approach

G. Medellín[1,2], J. A. Brinkkemper[3], A. Torres-Freyermuth[2], C. M. Appendini[2], E. T. Mendoza[2], and P. Salles[2]

[1]Cátedras-CONACyT, Consejo Nacional de Ciencia y Tecnología, México, D. F., Mexico
[2]Laboratorio de Ingeniería y Procesos Costeros, Instituto de Ingeniería, Universidad Nacional Autónoma de México, Sisal, Yucatán, Mexico
[3]Department of Physical Geography, Faculty of Geosciences, Utrecht University, Utrecht, the Netherlands

Received: 14 April 2015 – Accepted: 20 April 2015 – Published: 7 May 2015

Correspondence to: G. Medellín (gmedellinm@iingen.unam.mx)

Published by Copernicus Publications on behalf of the European Geosciences Union.

Abstract

We present a downscaling approach for the study of wave-induced extreme water levels at a location on a barrier island in Yucatan (Mexico). Wave information from a 30 year wave hindcast is validated with in situ measurements at 8 m water depth. The Maximum Dissimilarity Algorithm is employed for the selection of 600 representative cases, encompassing different wave characteristics and tidal level combinations. The selected cases are propagated from 8 m water depth till the shore using the coupling of a third-generation wave model and a phase-resolving non-hydrostatic Nonlinear Shallow Water Equations model. Extreme wave runup, $R_{2\,\%}$, is estimated for the simulated cases and can be further employed to reconstruct the 30 year period using an interpolation algorithm. Downscaling results show runup saturation during more energetic wave conditions and modulation owing to tides. The latter suggests that the $R_{2\,\%}$ can be parameterized using a hyperbolic-like formulation with dependency on both wave height and tidal level. The new parametric formulation is in agreement with the downscaling results ($r^2 = 0.78$), allowing a fast calculation of wave-induced extreme water levels at this location. Finally, an assessment of beach vulnerability to wave-induced extreme water level is conducted at the study area by employing the two approaches (reconstruction/parametrization) and a storm impact scale. The 30 year extreme water level hindcast allows the calculation of beach vulnerability as a function of return periods. It is shown that the downscaling-derived parameterization provides reasonable results as compared with the numerical approach. This methodology can be extended to other locations and can be further improved by incorporating the storm surge contributions to the extreme water level.

NHESSD
3, 3077–3117, 2015

1 Introduction

The assessment of beach vulnerability in low-lying areas is important for coastal managers and decision makers. Furthermore, these coastal systems are particularly sensitive to climate change effects, such as mean sea level increase and storm intensification (Wong et al., 2014). Thus, it is anticipated that low-lying areas will experience more severe coastal flooding and beach erosion during the following decades.

The beach vulnerability can be estimated by comparing extreme water level elevations to those of the beach morphology features (Sallenger, 2000). For instance, the storm impact scale proposed by Sallenger (2000) couples the fluid forcing and the beach morphology, by examining the relationship between the dune height and the water level due to the storm surge, wave setup, and extreme runup. This approach was validated in Stockdon et al. (2007) for a stretch of coast in North Carolina. Stockdon et al. (2007) employed lidar-derived measures of pre-storm dune and berm elevation and hurricane-induced water levels to hindcast the potential storm impact regime to the landfalls of Hurricane Bonnie (1998) and Hurricane Floyd (1999), which were further compared to the observed response. More recently, long-term observations were employed together with a runup parameterization in order to determine the return periods correlated to the storm impact scale in the coast of Oregon (Serafin and Ruggiero, 2014).

A great effort has been devoted to the development of methodologies for storm surge estimation (e.g. Lin et al., 2010; Irish et al., 2011). However, less attention has been given to the development of reliable approaches for the estimation of wave-induced runup. Wave runup is often calculated using parameterizations based on field observations (e.g. Ruessink et al., 1998; Ruggiero et al., 2001, 2004; Stockdon et al., 2006; Senechal et al., 2011). However, their performance is questionable during extreme wave conditions (Stockdon et al., 2014). Furthermore, runup parameterizations are strongly dependent on the beach morphology features, tidal level elevation, and wave

NHESSD
3, 3077–3117, 2015

forcing conditions. Therefore, a universal runup parameterization is not available and site-specific parameterizations should be developed.

The advent of nonlinear phase-resolving wave transformation numerical models allows the simulation of wave runup in a wave-by-wave basis. Different approaches have been developed with different degree of sophistication, including Nonlinear-Shallow Water Equations (NLSWE) models (e.g. Kobayashi and Wurjanto, 1992; Raubenheimer and Guza, 1996; Zijlema et al., 2011), Boussinesq-type models (e.g. Wei et al., 1999; Chen et al., 2003), Reynolds-Averaged Navier–Stokes models (e.g. Lin and Liu, 1998; Losada et al., 2008), and Large Eddy Simulation (Christensen, 2006; Zhou et al., 2014) models. The capabilities of more sophisticated approaches for addressing the study of small-scale processes demand higher computational cost. Non-hydrostatic NLSWE models (e.g. SWASH) allow to overcome some of the limitations in classic NLSWE models by incorporating wave dispersion in the simulations. This numerical approach has been employed for the study of extreme water levels on a fringing reef lagoon (e.g. Torres-Freyermuth et al., 2012), wave runup on beaches (e.g. Ruju et al., 2014; Guimarães et al., 2015), and infragravity shoreline dissipation (e.g. de Bakker et al., 2014). Furthermore, the potential for the runup parameterization has been shown in Brinkkemper et al. (2013).

The characterization of small-scale coastal processes such as runup from long-term datasets requires the implementation of a statistical method. Downscaling of wave conditions for the study of nearshore processes is possible through data reduction using a rigorous statistic approach (Camus et al., 2011a; Guanche et al., 2013). Camus et al. (2011a) employed a hybrid downscaling methodology to transfer wave climate to coastal areas. They show that interpolating simulated results using a Radial Basis Function provides good estimates to characterize a complete year of hourly sea states, and that the decrease of the error is negligible considering a subset of cases. This methodology was further extended to reconstruct time series of stability parameters on vertical breakwaters by Guanche et al. (2013). Therefore, combining numerical models

NHESSD
3, 3077–3117, 2015

with statistical methods provides a mean to characterize coastal dynamics reducing the computational cost.

The aim of this work is to present a methodology for the assessment of wave-induced vulnerability at a location on a barrier island located in Yucatan (Mexico). The methodology combines numerical, statistical, and probabilistic methods for the estimation of wave-induced water levels associated to return periods. Moreover, this approach allows the derivation of a site-specific runup parameterization for the study area. The outline of this paper is the following. Firstly, the study area location and characteristics are described in Sect. 2. The methodology for downscaling wave conditions in order to obtain a 30 year runup hindcast is presented in Sect. 3. Section 4 presents the reconstruction of the extreme water level time series and the derivation of a new runup parameterization. An assessment of beach vulnerability in the study area using reconstructed and parameterized results is presented in Sect. 5. Finally, concluding remarks and future work are presented (Sect. 6).

2 Study area

Dzilam de Bravo is located on a barrier island in the Northern Yucatan peninsula (Fig. 1). The coastline is fronted by a 200 km wide continental shelf with a very mild (1 : 1000) beach slope (Enriquez et al., 2010). The tidal regime is micro-tidal and wave conditions in the study area are dominated by local sea-breezes and meso-scale meteorological (cold-fronts) events known as *Nortes* (Appendini et al., 2013). Furthermore, less frequent hurricane events can also affect the study area. According to Mendoza et al. (2013), the Yucatan coast is more vulnerable to flood than to erosion during the impact of storms. Dzilam de Bravo is characterized by submarine dune fields (Cuevas et al., 2013) that induce a complex nearshore wave transformation. Cuevas et al. (2013) characterized the submarine dunes by means of sub-bottom seismologic profiles, finding at Dzilam de Bravo a mean dune height ranging from 0.8 to 1.0 m and a mean dune wave length of 98–120 m, predominantly moving northwestward. These sedimentary

NHESSD
3, 3077–3117, 2015

deposits (see Fig. 2) might play an important role in wave energy dissipation, providing a natural protection from storms to this site.

The beach profile at Dzilam de Bravo was measured using a DGPS system and extended landward with terrestial LIDAR information acquired in 2011. Moreover, the beach profile was further extended offshore to a water depth of 10 m assuming an equilibrium profile according to Dean (1991). Wave information at 8 m water depth is available from a 30 year hindcast (1979–2008) for the Gulf of Mexico and the Western Caribbean Sea (Appendini et al., 2014). These data was estimated by means of a third-generation spectral model forced with wind data from the North American Regional Reanalysis, NARR (Mesinger et al., 2006). The numerical model was calibrated/validated in deep waters with wave buoys (Appendini et al., 2013) and altimeter information (Appendini et al., 2014). Data measured with an ADCP located near the study area, between Chuburná and Yucalpetén (see Fig. 1), at approximately 8.5 m water depth was available for a 2.5 year period (June 2010–December 2012). Comparison of the in situ data and wave hindcast information (NODE12972, Fig. 1) presents good correlation between the model and observations for $H_s \lesssim 1$ m (see Fig. 3). The model underestimates H_s for values between 1.2 and 1.7, whereas hindcast data overestimates observations for $H_s \gtrsim 1.7$ m. However, an overall good agreement is observed between model and data. Thus, in this study a wave hindcast node located at approximately 10 m water depth in front of Dzilam de Bravo (NODE11583, Fig. 1) was selected as the offshore boundary condition (H_s, T_p, θ).

3 Methods

We extended a methodology to downscale wave information to the nearshore as proposed by Camus et al. (2011a) and Guanche et al. (2013) for the assessment of storm impact on barred beaches. The methodology is as follows. Firstly, a subset of wave conditions is selected from the three-hourly 30 year wave hindcast. Then, the selected sea states, with the corresponding tidal level, are propagated from deep waters until the

NHESSD
3, 3077–3117, 2015

shore employing numerical models. Extreme runup is computed and further employed for calculating a 30 year runup hindcast by means of interpolation. Subsequently, the 30 year runup information was employed in order to derive a runup parameterization for the study area. Finally, the storm impact for different return periods can be obtained using both numerical results and the new parameterization.

3.1 Selection of wave conditions

The available 30 year wave hindcast (Appendini et al., 2014) consists of a total of 87 664 sea states (H_s, T_p, and θ), one every three hours. Due to the computational effort involved to downscale the complete dataset for all sea states, it is desirable to obtain a representative subset. A comparison of selection algorithms applied for the analysis of wave climate is presented in Camus et al. (2011b). They found that the subset of wave conditions obtained by implementing the Maximum Dissimilarity Algorithm (MDA) was representative of the variety of sea states and therefore appropriate for downscaling wave climate.

The aim of the MDA, described in detail in Camus et al. (2011a, b), and Guanche et al. (2013) for coastal engineering applications, is to identify the most dissimilar subset of multivariate vectors (i.e. wave parameters) in a database. Therefore, the extracted subset of $\boldsymbol{M}$ vectors represents the diversity of the dataset consisting of N n-dimensional vectors. In this study, the multivariate data include significant wave height, H_s, peak period, T_p, mean wave direction, θ_m and mean sea level, Z_m. Wave parameters were obtained from the wave hindcast, while the timeseries of sea level corresponds to the astronomical tide prediction for this area (http://predmar.cicese.mx) during the same time period.

Following the procedure described in Camus et al. (2011a) and Guanche et al. (2013), the multivariate data at deep water are defined as,

$$X_i^* = H_{s,i}, T_{p,i}, \theta_{m,i}, Z_{m,i}; i = 1 \ldots, N \quad (1)$$

NHESSD
3, 3077–3117, 2015

where N corresponds to the 87 664 sea states from the 30 year wave hindcast. The first step in the methodology described in Camus et al. (2011a) is to normalize the vector components so they can be evenly weighted in the similarity criterion, defined by the Euclidean distance. Special consideration should be made for the circular variable (direction) when it is adapted to a linear scale, since it is recorded in a continuous scale where 0 and 360° are identical. Therefore, the circular distance should be implemented in that case where the maximum distance in the circle is equal to π. The sample data consisting of N dimensionless vectors is defined as

$$X_i = H_i, T_i, \theta_i, Z_i; i = 1 \ldots, N \tag{2}$$

from which a set of $\boldsymbol{M}$ vectors $D_1 \ldots D_M$ is selected by means of the MDA.

The selection starts by transferring one vector from the data sample to the subset D. Then, the rest of the $\boldsymbol{M} - 1$ vectors are selected calculating the dissimilarity between each of the reimaining elements in the database and the elements in the subset, transferring the most dissimilar one to the subset, considering the MaxMin version of the algorithm as proposed by Camus et al. (2011a). This procedure is repeated iteratively until the M elements are selected.

For instance, having a subset of $R (R \leq M)$, the dissimilarity among vector $\boldsymbol{i}$ of the data sample $N - R$ and the $\boldsymbol{j}$ vectors of the R subset is determined as,

$$d_{ij} = \|X_i - D_j\|; \boldsymbol{i} = 1, \ldots, N - R; \boldsymbol{j} = 1, \ldots, R. \tag{3}$$

Then, the dissimilarity between vector $\boldsymbol{i}$ and subset R, $d_{i,\text{subset}}$, is obtained as

$$d_{i,\text{subset}} = \min\|X_i - D_j\|; \boldsymbol{i} = 1, \ldots, N - R; \boldsymbol{j} = 1, \ldots, R. \tag{4}$$

Now, having calculated the $N - R$ dissimilarities, the following data to be selected is the one with the maximum $d_{i,\text{subset}}$. In this work, the Euclidean distance was computed using the DistanceMatrix algorithm developed by Fasshauer (2007), modified for the

NHESSD
3, 3077–3117, 2015

case of the directional parameters considering the circular distance as described in Camus et al. (2011a) and given by the following expression,

$$\|X_i - D_j\| = \sqrt{\left(\left(H_i - H_j^D\right)^2 + \left(T_i - T_j^D\right)^2 + \left(Z_i - Z_j^D\right)^2 + \left(\min\left(|\theta_i - \theta_j^D|, 2 - |\theta_i - \theta_j^D|\right)^2\right)}. \quad (5)$$

The final step is to denormalize the selected subset using,

$$D_j^* = H_{s,j}^D, T_{s,j}^D, \theta_{s,j}^D, Z_{s,j}^D; j = 1, \ldots, M. \quad (6)$$

Here, a total of $M = 600$ sea states were selected, which adequately represent the whole sample and their distribution uniformly covers the area of the input data as well as its borders (Fig. 4). It is also worth to consider that the selected sea states are well distributed along the time series of wave parameters and sea level (Fig. 7).

3.2 Propagation of selected wave conditions

Wave propagation from 8 m water depth until the shoreline was performed employing the coupling of a spectral wave model (SWAN; Booij et al., 1999) and a phase-resolving nonlinear non-hydrostatic model (SWASH; Zijlema et al., 2011). The SWAN (Simulating WAves Nearshore) model is a third-generation wave model for coastal regions, based on a Eulerian formulation of the discrete spectral balance of action density, which accounts for wind generation, whitecapping, triad and quadruplet wave–wave interactions, bottom friction, and wave-induced wave breaking (Booij et al., 1999). On the other hand, the SWASH (Simulating Waves till Shore) model employs the nonlinear shallow water equations, including terms for non-hydrostatic pressure, which makes the model suitable for simulating wave transformation due to nonlinear wave–wave interactions in both surf and swash zones, wave-current interaction, wave breaking, and wave run-up. Wave breaking is included in the model based upon the bore formation

NHESSD
3, 3077–3117, 2015

concept. Flooding and drying of grid cells is important for a correct run-up simulation. In this model, no special features are needed to model dry cells accurately if the time step is chosen correctly, as flooding never happens faster than one grid size per time step (Zijlema et al., 2011).

The SWAN model is run in stationary one-dimensional mode (mesh size 1 m) along the section from 8 to 4 m water depth and forced with a Jonswap spectrum at the offshore boundary. The wave energy spectrum at 4 m depth calculated by the SWAN model is employed as the seaward boundary forcing for the SWASH model (Fig. 5). The SWASH domain extends from 4 m water depth to the shoreline with a mesh size of 0.1 m. The initial time step is 0.025 s with a maximum Courant number of 0.5. Simulations were sampled for 2170 s, after 530 s of spin up time.

3.3 Model data analysis: extreme water level calculation

The instantaneous water level elevation, $\eta(t)$, relative to mean sea level was extracted from the SWASH simulations for each sea state propagated as the height of the bottom profile at the location of the wet–dry interface with respect to time (Fig. 6a). This location was tracked as the first grid point in which the water depth was less than 0.005 m in order to obtain a continuous time series. Subsequently, the extreme runup was calculated from the runup maxima (R) following the work by Stockdon et al. (2006), as the 2 % exceedence value (Fig. 6b). Additionally, the mean value of the wave runup time series ($<\eta>$), which corresponds to a super-elevation of the mean water level due to the presence of waves known as the wave setup (Longuet-Higgins and Stewart, 1964), was obtained for each case. Following Sallenger (2000) and Stockdon et al. (2007) we define the extreme water levels $R_{\text{high}} = R_{2\,\%} + Z$ and $R_{\text{low}} = <\eta> + Z$ for each simulated case.

NHESSD
3, 3077–3117, 2015

3.4 Reconstruction of the extreme water level (R_{high}) time series: RBF interpolation

The extreme water level, R_{high} and R_{low}, associated with each of the 600 selected sea states were employed to reconstruct the 30 year long time series. Notice that the storm surge is not included in Z for this work but can be incorporated. The extreme water level time series reconstruction is performed by means of an interpolation technique based on the Radial Basis Functions (RBF). This is an exact interpolation technique, given that the interpolated surface always passes exactly through the data points, and is suitable for multivariate scattered data interpolation. Franke (1982) tested the performance of about 30 methods for scattered data interpolation, finding that the best and second best were methods based on RBF. This method has been previously implemented in diverse applications such as the reconstruction of topographic surfaces based on coordinate data (Hardy, 1971), and more recently, for the downscaling of wave parameters (Camus et al., 2011a; Guanche et al., 2013). Following the method presented in Camus et al. (2011a) and considering that $X_i = \{H_{si}, T_{pi}, \theta_{mi}, Z_i\}; i = 1, \ldots, N$ represents each sea state in the 30 year long time series and $D_j = \{H^D_{sj}, T^D_{pj}, \theta^D_{mj}, Z^D_j\}; j = 1, \ldots, M$ represents each one of the $M = 600$ selected cases associated with a value of R_{high}, the interpolation function is given by:

$$\mathrm{RBF}(X_i) = p(X_i) + \sum_{j=1}^{M} a_j \Phi(\|X_i - D_j\|) \tag{7}$$

where Φ is the radial basis function, $\|.\|$ denotes the Euclidean norm, $p(X_i) = b_0 + b_1 H_{si} + b_2 T_{pi} + b_3 \theta_{mi} + b_4 Z_i$, and Φ is a Gaussian function defined as,

$$\Phi\|X_i - D_j\| = \exp\left(-\frac{\|X_i - D_j\|^2}{2c^2}\right) \tag{8}$$

where the points $D_j, j = 1, \ldots, M$ are the centers of the RBF approximation and c is a shape parameter that must be carefully selected since it has a strong influence on

NHESSD
3, 3077–3117, 2015

the accuracy of the solution (Rippa, 1999). The interpolation based on RBF was performed by means of an algorithm developed by Fasshauer (2007) which incorporates the algorithm proposed by Rippa (1999) for the selection of an optimal value for the shape parameter c. The selection is performed by minimizing the RMS error of a data fit based on a radial interpolant for which one of the centers was left out (*leave-one-out cross validation* approach).

The coefficients b of the monomials and the coefficients a of the RBF are obtained by the interpolation conditions (Camus et al., 2011a):

$$\mathrm{RBF}(D_j) = f_j(D_j) = D_{\mathrm{p},j}; j = 1, \ldots, M \tag{9}$$

where $D_{\mathrm{p},j}$ are the real functions defined by the calculated extreme water level values R_{high} which correspond to the M selected sea states (D_j).

Subsequently, the R_{high} time series can be reconstructed for the 30 year period by means of the RBF as follows (see bottom panel of Fig. 7),

$$R_{\mathrm{high},i} = \mathrm{RBF}_{R_{\mathrm{high}}}(\{D_j, R_{\mathrm{high},j}(j = 1, \ldots, M)\}, X_i) \tag{10}$$

where $i = 1, \ldots, N$.

Similarly, the wave-induced mean water level time series, $R_{\mathrm{low}} = <\eta> + Z$, is reconstructed following the same methodology with $M = 600$.

Camus et al. (2011a) compared the reconstructed time series for a range of M values (i.e. $M = 25$, 100, and 1000) against simulated time series of $N = 8784$, finding that the error obtained in the estimation of wave parameters is almost negligible considering only $M = 100$ cases. Therefore, they recommend that for the specific application of transformation of wave climate from deep to shallow waters, $100 \leq M \leq 200$ is an adequate number of cases. Guanche et al. (2013) validated their interpolated values with those calculated analytically, finding that the reconstructed series with more than 100–200 cases out of 500 000 cases reached values of less than 1 % error, and with 500 cases the error made is almost negligible.

NHESSD
3, 3077–3117, 2015

In this work, a sensitive analysis on the dependency of R_{high} to the the number of cases employed for the reconstruction was conducted for M = 50, 100, 200, 300, 400, 500, 600. The mean and SD of each time series were computed, finding that for $M > 300$ cases, the variability of these statistic parameters is insignificant (not shown).

3.5 Runup parameterization

The reconstructed 30 year extreme water level time series provides a mean to correlate $R_{2\,\%}$ to offshore wave conditions. The runup is obtained by subtracting the astronomical tide Z from R_{high} for each case. Different runup parameterizations from the literature (Ruggiero et al., 2001; Senechal et al., 2011) were employed and calibrated using the downscaled data. Furthermore, due to the observed modulation of runup by tides (e.g. Guedes et al., 2011), a new parameterization of runup and setup was derived for the study area as a function of the tidal level and wave conditions employing the 30 year $R_{2\,\%}$ data.

3.6 Extreme value analysis of R_{high} and R_{low}

In order to incorporate the probability to a given extreme water level, the annual maxima of R_{high} and R_{low} were fitted to the Generalized Extreme Value (GEV) distribution of Jenkinson (1955), which has been widely employed for modelling extremes of natural phenomena. The GEV distribution is given by,

$$F(x;k,\mu,\sigma) = \exp[-\{1-k(x-\mu)/\sigma\}^{1/k}], \quad k \neq 0, \tag{11}$$

$$= \exp[-\exp\{-(x-\mu)/\sigma\}], \quad k = 0, \tag{12}$$

where μ and σ are the location and scale parameters, respectively, and the shape parameter k determines which extreme-value distribution is represented: Gumbel ($k = 0$), Fréchet ($k > 0$), and Weibull ($k < 0$). WAFO-group (2000) toolbox was used for the GEV model, in which the the parameter estimation methods used are the Maximum Likelihood (ML) method (Prescott and Walden, 1980) and the Probability-Weighted Mo-

NHESSD
3, 3077–3117, 2015

ments (PWM) method (Hosking et al., 1985). The latter was selected for parameter estimation since it is more suitable for small samples (N = 15, 25) (Hosking et al., 1985), and resulted in a better goodness of fit to the annual maxima data. The estimated parameters for R_{high} yearly maxima are the shape parameter k = 0.3057 with a 95 % confidence interval, and a location and scale parameters estimated to μ = 1.5739 and σ = 0.1238. Regarding the R_{low} annual maxima data, the estimated parameters are k = 0.3184, μ = 0.7247, and σ = 0.0896.

3.7 Storm impact scale

A storm impact scale for barrier islands that considers the magnitude of fluid forcing (storm induced water-levels) relative to beach morphology (dune/berm elevation) was first proposed by Sallenger (2000). The model defines four storm-impact regimes depending on the relative relationship between the sand dune or beach berm elevation and the storm-induced water levels. Sallenger (2000) defines the elevation measures that determine the four impact regimes. The first elevation measure, slightly modified in Stockdon et al. (2007) as R_{low} is equal to the sum of storm surge, astronomical tide, and wave setup. A second elevation measure, R_{high}, incorporates the contributions of astronomical tide, storm surge, and the 2 % exceedence level for vertical wave runup R_2 % which in turn includes setup and swash (Sallenger, 2000). The topographic elevation measures correspond to the dune crest, D_{high}, and the dune toe, D_{low}, as depicted in Fig. 2.

The four impact regimes described in Sallenger (2000) and Stockdon et al. (2007) are: (i) *swash*, (ii) *collision*, (iii) *overwash*, and (iv) *inundation*. In the *swash* regime ($R_{high} < D_{low}$), wave runup is limited to the foreshore region and the eroded sand during storms is generally transported offshore until it returns to the beach during calm periods, while in the *collision* regime ($D_{high} > R_{high} > D_{low}$) wave runup collides with the dune base causing more long-lasting erosion where the sediment transported offshore usually does not return and dunes may be rebuilt by slower aeolian processes. When the *overwash* $R_{high} > D_{high}$ regime occurs, runup overtops the dune and sand

NHESSD
3, 3077–3117, 2015

is transported landward and does not immediately return seaward to the beach under post-storm conditions. The fourth and most severe regime is *inundation* ($R_{low} > D_{high}$) when the maximum water level is sufficient to completely submerge the barrier island and it is suggested, based on limited observations, that massive net onshore transport and landward migration of sand bodies might occurr (Sallenger, 2000).

The results of the extreme value analysis of R_{high} and R_{low} for different return periods where correlated with the beach morphology features (i.e. D_{high} and D_{low}) derived from the LIDAR data.

4 Results

The 30 year time series of R_{high} (Fig. 7) and R_{low} (not shown) reconstructed by means of the RBF interpolation of the simulated cases are further employed for the parameterization of runup and setup, and an assessment of the vulnerability of the beach by means of the storm impact scale proposed by Sallenger (2000).

4.1 Runup parameterization

Beach vulnerability is often evaluated using runup parameterizations (e.g. Stockdon et al., 2007; Serafin and Ruggiero, 2014). Therefore, the development of suitable parameterizations is important for vulnerability studies. The extreme runup results, obtained from the reconstructed extreme water level, are further analyzed in terms of their relationship with offshore wave parameters, beach conditions, and astronomical tide. For that purpose, the 5 % exceedance value of water level according to the astronomical tide Z was found for high ($Z \geq Z_{5\,\%} = 0.32$ m) and low water water level ($Z \leq Z_{5\,\%} = -0.32$ m), while for the mean water level the values considered were $0.05 \geq Z \geq -0.05$ m. Analyzing the behavior of the $R_{2\,\%}$ and $< \eta >$ values it was clear that they are modulated/saturated by the tides/wave energy conditions. Firstly, a linear relationship for $R_{2\,\%}$ is employed, as proposed by Ruggiero et al. (2001),

NHESSD
3, 3077–3117, 2015

which depends on deepwater wave parameters (H_s,$L_0 = gT^2/2\pi$) and beach slope, S. Deepwater wave parameters correspond to the wave hindcast data, while the value of $S = 0.09$ was considered according to Brinkkemper et al. (2013). This parametrization describes remarkably well the behavior of the values corresponding to high water level ($Z \geq Z_{5\%} = 0.32$ m, darker grey dots in Fig. 8a) and is very similar to the best fit (zero intercept) to the data associated to high water (solid line). Furthermore, a relationship obtained on a previous study (Brinkkemper et al., 2013) performed on the same area but employing the results of only five simulations, corresponding to energetic wave conditions associated to high water level (Fig. 8a, dash-dot line), is almost identical to the one obtained on this study for all values corresponding to high water level (Fig. 8a, solid line). Even though the r^2 value of the linear fit (zero intercept) is satisfactory ($r^2 = 0.87$) for the case of high water level, this linear relationships are only valid up to a value ($1.1 \lesssim R_{2\%} \lesssim 1.3$ m) where saturation in maximum runup values is observed for more energetic conditions ($(SH_sL_0)^{1/2} \gtrsim 4$ m). The linear fit performed to the whole data set (dotted line) showed a lower r^2 value and a higher rmse (see Table 1). Regarding the setup values, the linear parametrization proposed by Stockdon et al. (2006) is employed, which includes the deepwater wavelength, $L_0(T_0)$, and the foreshore slope, β_f. This formulation lays on the upper limit of the data (Fig. 8b, dashed line), better describing the values associated to high water even though it differs from the linear fit (zero intercept) to those values. The r^2 corresponding to the linear fit associated to high water values is greater than the one obtained considering the whole data set. Similarly to runup values, saturation and a dependency on water level is observed for setup values. The saturation value for setup associated to high water level is around 0.35 m.

Due to the observed saturation of runup and setup values associated to the water level (astronomical tide), a more suitable hyperbolic–like relationship is employed. This saturation was previously examined by Brinkkemper et al. (2013) following the relationship proposed by Senechal et al. (2011). It was found that for $H_s \gtrsim 1.5$ m the saturation value of $R_{2\%}$ varies accordingly with water level (Fig. 9). Therefore, an hyperbolic tan-

NHESSD
3, 3077–3117, 2015

gent relationship was fitted through the method of least squares separating the data in high ($Z \geq Z_{5\%} = 0.32$ m), mean ($0.05 \geq Z \geq -0.05$ m), and low ($Z \leq Z_{5\%} = -0.32$ m) water level. For each set of data a hyperbolic tangent fit was performed (Fig. 9) obtaining acceptable values of r^2 and rmse (Table 2). The relationship proposed by Senechal et al. (2011) falls on the upper limit of the data corresponding to high water level. The tanh argument of the relationship presented in Senechal et al. (2011) and the one obtained in this study for high water level is almost the same ($0.39H_0$ and $0.4H_0$) and very similar to the one obtained by Brinkkemper et al. (2013) of $0.5H_0$. However, the saturation value in the case of Senechal et al. (2011) is much higher (2.14 m) than the one obtained by Brinkkemper et al. (2013) of 1.62 m which is exactly the same as the one obtained in the present study.

Thus, in order to obtain a generalized expression for the prediction of the 2 % exceedence value of runup ($R_{2\%}$) and setup ($<\eta>$) as a function of H_0 and Z, a simple linear relationship was fitted to the hyperbolic tangent fit parameters, a and b (Table 2), with r^2 values of 0.99 and 0.95 respectively in the case of the runup fit and 0.97 and 0.63 for setup fit parameters. The generalized expression obtained for $R_{2\%}$ is given by

$$R_{2\%} = a \cdot \tanh(b \cdot H_0) \tag{13}$$

where H_0 is the deep water wave height, $a = 1.615Z + 1.098$ and $b = -0.297Z + 0.476$ m. A similar expression was obtained for the case of the setup, with $a = 0.23Z + 0.27$ and $b = 0.15Z + 0.46$.

The runup and setup were calculated with the linear and the generalized expressions, the latter depending only on the deep water wave height and the astronomical tide. The values obtained through the linear parameterization showed a greater dispersion for more energetic conditions with respect to the values obtained using the hyperbolic parameterization, due to the saturation of wave runup not accounted for on the linear relationship, showing a correlation of 0.73 with respect to the reconstructed runup values (Fig. 10a). Regarding the hyperbolic parameterization, the parameterized values were compared to the reconstructed values obtaining, for the case of the

NHESSD
3, 3077–3117, 2015

$R_{2\,\%}$, an r^2 value of 0.78 considering the whole set and an $r^2 = 0.86$ considering only the waves approaching from the North (NNW,N,NNE), $22.5 > \theta > 337.5$ (Fig. 10b). Regarding the setup, $< \eta >$, the correlation obtained for the whole data set is 0.75, and 0.86 for the data associated to waves arriving from the North (not shown). For both cases, $R_{2\,\%}$ and $< \eta >$ the dispersion is greater for smaller values, $R_{2\,\%} \lesssim 0.5$ m and $< \eta > \lesssim 0.1$ m, and for waves arriving with an angle $22.5 < \theta < 337.5$.

The overall modulation of runup and setup (not shown) due to wave height and astronomical tide is captured by the generalized hyperbolic parametrization and better illustrated in the reconstructed vs. parameterized runup timeseries (Fig. 10c). Some deviations are observed but the general behaviour is reproduced satisfactorily as compared to the linear parametrization where overestimation of runup maxima is observed and the modulation of the runup due to tides is not well captured (Fig. 10c, dashed line).

4.2 Extreme water level

The reconstruction of the 30 year extreme water level allows us to determine the corresponding return periods. In order to do that, a Generalized Extreme Value (GEV) distribution is fitted to the 30 year (reconstructed) R_{high} time series. Figure 11 shows the return level extrapolation of R_{high} for 100 years return period with the 95 % confidence bounds ($100 \cdot (1 - \alpha)$, $\alpha = 0.05$). Similarly, the extreme analysis for R_{low} can be performed. These parameters can be employed in order to associate the storm impact scale to a given return period (e.g. Serafin and Ruggiero, 2014). Additionaly, the same procedure was followed for the parameterized values of $R_{2\,\%}$ obtained by the generalized expression described in the previous section, incoporating the contribution of Z to obtain the R_{high} and R_{low} 30 year time series.

The values of R_{high} associated to a 5, 10, 50, and 100 years return period obtained from the reconstructed timeseries are smaller than the ones predicted from the parameterized timeseries for all return periods (Table 3). However, the R_{low} values predicted

NHESSD
3, 3077–3117, 2015

from the reconstructed timeseries are greater than the parameterized R_{low} values (Table 4) for all return periods (5, 10, 50, and 100 years).

5 Discussion: beach vulnerability assessment on a barrier island

Using the 30 year long time series of R_{high} = astronomical tide + $R_{2\%}$ (missing surge) and R_{low} = astronomical tide+ $<\eta>$ (missing surge), obtained by means of both the RBF interpolation and the parameterizations, together with the available LIDAR information, from which the topographic elevations (D_{high} (dune crest) and D_{low} (dune toe) were extracted (Fig. 2), the storm impact regimes can be estimated.

Based on the return values of R_{high} and R_{low} (Tables 3 and 4) corresponding to a 5, 10, 50, and 100 years return period, the associated storm impact regime *collision* ($D_{high} > R_{high} > D_{low}$) was found (Table 5). This regime would occur even if the storm surge is not considered causing long lasting-erosion and the possibility of sediment not returning from offshore. However, considering a typical storm surge elevation of ≈ 0.5 m associated to the frequent cold fronts in the study area in addition to the mean return values of R_{high} would result in water elevations that would exceed the dune crest for a return period of 10 years or more (Table 5, Fig. 11), leading to the *overwash* $R_{high} > D_{high}$ storm impact regime, where runup overtops the dune and the sand transported landward does not return seaward to the beach under post-storm conditions.

The storm impact scale is a valuable tool for predicting coastal response to storms (with an accuracy that depends on the regime) as well as to analyze the longshore variability of coastal change in a stretch of coast (Stockdon et al., 2007). However, in this work, the longshore variability is not evaluated since a single beach profile is considered. Future work will be devoted to include other sites in order to explore the variability along the northern Yucatan coast and the contribution of the storm surge to the extreme water levels in this area. Furthermore, effects due to sea level rise and storm intensification must be considered.

NHESSD
3, 3077–3117, 2015

6 Conclusions

We present a downscaling approach for the study of wave runup and beach vulnerability on a barrier island. Wave conditions from a 30 year wave hindcast are propagated till the shore using a third generation wave model coupled with a NLSWE non-hydrostatic mode in order to calculate the extreme runup. The numerical results allow us to reconstruct the 30 year time series to be further employed for parameterization of runup in this area. A new runup parameterization which incorporates saturation and tidal modulation is derived and compared with the numerical results. The 30 year extreme water levels are employed for a probabilistic assessement of beach vulnerability at a location on a barrier island in Yucatan. Both downscaling results and the runup parameterization provided similar results for different return periods. Field evidence suggests the importance of incorporating storm surge estimations for a more reliable analysis of beach vulnerability in this area.

Acknowledgements. First author is funded by the National Council of Science and Technology through project Cátedras-CONACyT 1146. We appreciate the support provided by the Institute of Engineering – UNAM through the International Projects 4314 and 4320. Many thanks to José López González for field support and data adquisicion. J. A. Brinkkemper is financed by the Dutch Technology Foundation STW, which is part of the Dutch Organisation for Scientific Research (NWO) and partly funded by the Ministry of Economic Affairs (project number 12397). A. Torres-Freyermuth acknowledges financial support provided by DGAPA UNAM (PAPIIT IN107315). Finally, we acknowledge Delft University of Technology for making the development of SWASH possible.

NHESSD
3, 3077–3117, 2015

References

Appendini, C. M., Torres-Freyermuth, A., Oropeza, F., Salles, P., Lopez, J., and Mendoza, E. T.: Wave modeling performance in the Gulf of Mexico and western Caribbean: wind reanalyses assessment, Appl. Ocean Res., 39, 20–30, doi:10.1016/j.apor.2012.09.004, 2013. 3081, 3082

Appendini, C. M., Torres-Freyermuth, A., Salles, P., Lopez, J., and Mendoza, E. T.: Wave climate and trends for the Gulf of Mexico: a 30-yr wave hindcast, J. Climate, 27, 1619–1632, doi:10.1175/JCLI-D-13-00206.1, 2014. 3082, 3083

Booij, N., Ris, R. C., and Holthuijsen, L. H.: A third generation wave model for coastal regions; part 1: model description and validation, J. Geophys. Res., 104, 7649–7666, 1999. 3085

Brinkkemper, J. A., Torres-Freyermuth, A., Mendoza, E. T., and Ruessink, B. G.: Parameterization of wave run-up on beaches in Yucatan, Mexico: a numerical study, Coast. Dynam., 25, 225–234, 2013. 3080, 3092, 3093, 3114, 3115

Camus, P., Mendez, F. J., and Medina, R.: A hybrid efficient method to downscale wave climate to coastal areas, Coast. Eng., 58, 851–862, doi:10.1016/j.coastaleng.2011.05.007, 2011a. 3080, 3082, 3083, 3084, 3085, 3087, 3088

Camus, P., Mendez, F. J., Medina, R., and Cofiño, A. S.: Analysis of clustering and selection algorithms for the study of multivariate wave climate, Coast. Eng., 58, 453–462, doi:10.1016/j.coastaleng.2011.02.003, 2011b. 3083

Chen, Q., Kirby, J. T., Dalrymple, R. A., Shi, F., and Thornton, E. B.: Boussinesq modeling of longshore currents, J. Geophys. Res., 108, 3362, doi:10.1029/2002JC001308, 2003. 3080

Christensen, E. D.: Large eddy simulation of spilling and plunging breakers, Coast. Eng., 53, 463–485, 2006. 3080

Cuevas, E., Liceaga-Correa, M. A., Rincón-Sandoval, L. A., Mexicano-Cíntora, G., Arellano-Mendez, L., Euán-Ávila, J. I., Hernández-Núñez, H., and Mulsow, S.: Morphological and sedimentological assessment of submarine dune fields on the coast of Yucatan, Mexico, Cienc. Mar., 39, 83–99, doi:10.7773/cm.v39i1.2152, 2013. 3081

Dean, R. G.: Equilibrium beach profiles: characteristics and applications, J. Coastal Res., 7, 53–84, 1991. 3082

de Bakker, A., Tissier, M., and Ruessink, B.: Shoreline dissipation of infragravity waves, Cont. Shelf. Res., 72, 73–82, doi:10.1016/j.csr.2013.11.013, 2014. 3080

NHESSD
3, 3077–3117, 2015

Enriquez, C., Marino-Tapia, I. J., and Herrera-Silveira, J. A.: Dispersion in the Yucatan coastal zone: implications for red tide events, Cont. Shelf. Res., 30, 127–137, doi:10.1016/j.csr.2009.10.005, 2010. 3081

Franke, R.: Scattered data interpolation: test of some methods, Math. Comput., 38, 181–200, 1982. 3087

Fasshauer, G. F.: Meshfree Approximation Methods with MATLAB, World Scientific Publishing Co., Inc., River Edge, NJ, USA, 2007. 3084, 3088

Guanche, Y., Camus, P., Guanche, R., Mendez, F. J., and Medina, R.: A simplified method to downscale wave dynamics on vertical breakwaters, Coast. Eng., 71, 68–77, doi:10.1016/j.coastaleng.2012.08.001, 2013. 3080, 3082, 3083, 3087, 3088

Guedes, R. M. C., Bryan, K. R., Coco, G., and Holman, R. A.: The effects of tides on swash statistics on an intermediate beach, J. Geophys. Res.-Oceans, 116, C04008, doi:10.1029/2010JC006660, 2011. 3089

Guimarães, P. V., Farina, L., Toldo Jr., E., Diaz-Hernandez, G., and Akhmatskaya, E.: Numerical simulation of extreme wave runup during storm events in Tramandaí Beach, Rio Grande do Sul, Brazil, Coast. Eng., 95, 171–180, doi:10.1016/j.coastaleng.2014.10.008, 2015. 3080

Hardy, R. I.: Multiquadratic equations of topography and other irregular surfaces, J. Geophys. Res., 76, 1905–1915, 1971. 3087

Hosking, J., Wallis, J., and Wood, E.: Estimation of the generalized extreme-value distribution by the method of probability-weighted moments, available at: http://www.scopus.com/inward/record.url?eid=2-s2.0-0022113451&partnerID=40&md5=fc3264ad2179c3fe21f7c247dc79ff84 (last access: 27 November 2014), Technometrics, 27, 251–261, 1985. 3090

Irish, J. L., Song, Y. K., and Chang, K.-A.: Probabilistic hurricane surge forecasting using parameterized surge response functions, Geophys. Res. Lett., 38, L03606, doi:10.1029/2010GL046347, 2011. 3079

Jenkinson, A. F.: The frequency distribution of the annual maximum (or minimum) of meteorological elements, Q. J. Roy. Meteorol. Soc., 81, 158–171, 1955. 3089

Kobayashi, N. and Wurjanto, A.: Irregular wave setup and run-up on beaches, J. Waterw. Port Coast. Ocean Eng., 118, 368–386, 1992. 3080

Lin, N., Emanuel, K. A., Smith, J. A., and Vanmarcke, E.: Risk assessment of hurricane storm surge for New York City, J. Geophys. Res.-Atmos., 115, D18121, doi:10.1029/2009JD013630, 2010. 3079

NHESSD
3, 3077–3117, 2015

Lin, P. and Liu, P. L.-F.: A numerical study of breaking waves in the surf zone, J. Fluid Mech., 359, 239–264, 1998. 3080

Longuet-Higgins, M. S. and Stewart, R.: Radiation stress in water waves: a physical discussion with applications, Deep-Sea Res., 11, 529–562, 1964. 3086

Losada, I. J., Lara, J. L., Guanche, R., and Gonzalez-Ondina, J. M.: Numerical analysis of wave overtopping of rubble mound breakwaters, Coast. Eng., 55, 47–62, doi:10.1016/j.coastaleng.2007.06.003, 2008. 3080

Mendoza, E., Trejo-Rangel, M., Salles, P., Appendini, C., Gonzalez, J., and Torres-Freyermuth, A.: Storm characterization and coastal hazards in the Yucatan Peninsula, J. Coastal Res., 03/2013, 790–795, doi:10.2112/SI65-134.1, 2013. 3081

Mesinger, F., DiMego, G., Kalnay, E., Mitchell, K., Shafran, P., Ebisuzaki, W., Jović, D., Woollen, J., Rogers, E., Berbery, E., Ek, M., Fan, Y., Grumbine, R., Higgins, W., Li, H., Lin, Y., Manikin, G., Parrish, D., and Shi, W.: North American regional reanalysis, B. Am. Meteorol. Soc., 87, 343–360, doi:10.1175/BAMS-87-3-343, 2006. 3082

Prescott, P. and Walden, A.: Maximum likelihood estimation of the parameters of the generalized extreme-value distribution, Biometrika, 67, 723–724, 1980. 3089

Raubenheimer, B. and Guza, R. T.: Observations and predictions of run-up, J. Geophys. Res.-Oceans, 101, 25575–25587, doi:10.1029/96JC02432, 1996. 3080

Rippa, S.: An algorithm for selecting a good value for the parameter c in radial basin function interpolation, Adv. Comput. Math., 11, 193–210, 1999. 3088

Ruessink, B., Kleinhans, M., and den Beukel, P.: Observations of swash under highly dissipative conditions, J. Geophys. Res.-Oceans, 103, 3111–3118, 1998. 3079

Ruggiero, P., Komar, P. D., McDougal, W. G., Marra, J. J., and Beach, R. A.: Wave runup, extreme water levels and the erosion of properties backing beaches, J. Coast. Res., 17, 407–419, 2001. 3079, 3089, 3091, 3114

Ruggiero, P., Holman, R. A., and Beach, R. A.: Wave run-up on a high-energy dissipative beach, J. Geophys. Res.-Oceans, 109, C06025, doi:10.1029/2003JC002160, 2004. 3079

Ruju, A., Lara, J. L., and Losada, I. J.: Numerical analysis of run-up oscillations under dissipative conditions, Coast. Eng., 86, 45–56, doi:10.1016/j.coastaleng.2014.01.010, 2014. 3080

Sallenger, A. H.: Storm impact scale for barrier islands, J. Coastal Res., 16, 890–895, doi:10.1002/2014JC010093, 2000. 3079, 3086, 3090, 3091

NHESSD

3, 3077–3117, 2015

Senechal, N., Coco, G., Bryan, K. R., and Holman, R. A.: Wave runup during extreme storm conditions, J. Geophys. Res.-Oceans, 116, C07032, doi:10.1029/2010JC006819, 2011. 3079, 3089, 3092, 3093, 3115

Serafin, K. A. and Ruggiero, P.: Simulating extreme total water levels using a time-dependent, extreme value approach, J. Geophys. Res.-Oceans, 119, 6305–6329, doi:10.1002/2014JC010093, 2014. 3079, 3091, 3094

Stockdon, H. F., Holman, R. A., Howd, P. A., and Sallenger, A. H.: Empirical parameterization of setup, swash, and runup, Coast. Eng., 53, 573–588, doi:10.1016/j.coastaleng.2005.12.005, 2006. 3079, 3086, 3092, 3114

Stockdon, H. F., Sallenger Jr., A. H., Holman, R. A., and Howd, P. A.: A simple model for the spatially-variable coastal response to hurricanes, Mar. Geol., 238, 1–20, doi:10.1016/j.margeo.2006.11.004, 2007. 3079, 3086, 3090, 3091, 3095

Stockdon, H. F., Thompson, D., Plant, N., and Long, J.: Evaluation of wave runup predictions from numerical and parametric models, Coast. Eng., 92, 1–11, doi:10.1016/j.coastaleng.2014.06.004, 2014. 3079

Torres-Freyermuth, A., Mariño-Tapia, I., Coronado, C., Salles, P., Medellín, G., Pedrozo-Acuña, A., Silva, R., Candela, J., and Iglesias-Prieto, R.: Wave-induced extreme water levels in the Puerto Morelos fringing reef lagoon, Nat. Hazards Earth Syst. Sci., 12, 3765–3773, doi:10.5194/nhess-12-3765-2012, 2012. 3080

WAFO-group: WAFO – a Matlab Toolbox for Analysis of Random Waves and Loads – a Tutorial, Tech. rep., available at: http://www.maths.lth.se/matstat/wafo, last access: 11 November 2014, Math. Stat., Center for Math. Sci., Lund Univ., Lund, Sweden, 2000. 3089

Wei, G., Kirby, J. T., and Sinha, A.: Generation of waves in Boussinesq models using a source funcion methods, Coast. Eng., 36, 271–299, 1999. 3080

Wong, P. P., Losada, I. J., Gattuso, J.-P., Hinkel, J., Khattabi, A., McInnes, K. L., Saito, Y., and Sallenger, A.: Coastal systems and low-lying areas, in: Climate Change 2014: Impacts, Adaptation, and Vulnerability, Part A: Global and Sectoral Aspects, Contribution of Working Group II to the Fifth Assessment Report of the Intergovernmental Panel on Climate Change, edited by: Field, C. B., Barros, V., Dokken, D., Mach, K., Mastrandrea, M., Bilir, T., Chatterjee, M., Ebi, K., Estrada, Y., Genova, R., Girma, B., Kissel, E., Levy, A., MacCracken, S., Mastrandrea, P., and White, L., Cambridge University Press, Cambridge, UK and New York, NY, USA, 361–409, 2014. 3079

NHESSD
3, 3077–3117, 2015

Zhou, Z., Sangermano, J., Hsu, T.-J., and Ting, F. C. K.: A numerical investigation of wave-breaking-induced turbulent coherent structure under a solitary wave, J. Geophys. Res.-Oceans, 119, 6952–6973, doi:10.1002/2014JC009854, 2014. 3080

Zijlema, M., Stelling, G., and Smit, P.: SWASH: an operational public domain code for simulating wave fields and rapidly varied flows in coastal waters, Coast. Eng., 58, 992–1012, doi:10.1016/j.coastaleng.2011.05.015, 2011. 3080, 3085, 3086

NHESSD

3, 3077–3117, 2015

Table 1. Zero intercept linear regression to $R_{2\%}$ values with respect to $(SH_sL_0)^{1/2}$ and $<\eta>$ values with respect to $\beta_f(H_0L_0)^{1/2}$, considering the whole set of data and those associated to high water level ($Z \geq Z_{5\%} = 0.32$ m), correlation (r^2) and root mean square error (rmse) in meters.

	slope	r^2	rmse (m)
$R_{2\%all}$	0.1889	0.7135	0.11
$R_{2\%HWL}$	0.2442	0.8738	0.0976
$<\eta>_{all}$	0.1550	0.6513	0.0284
$<\eta>_{HWL}$	0.2217	0.7382	0.0335

NHESSD
3, 3077–3117, 2015

Table 2. Hyperbolic tangent fit to $R_{2\%}$ values, $R_{2\%} = a\tanh(bH_0)$, and $< \eta >$ values corresponding to high water level, mean water level, and low water level. Correlation (r^2) and root mean square error (rmse) in meters.

	a	b	r^2	rmse (m)
$R_{2\%HWL}$	1.62	0.39	0.859	0.103
$R_{2\%MWL}$	1.08	0.45	0.766	0.097
$R_{2\%LWL}$	0.59	0.58	0.642	0.057
$< \eta >_{HWL}$	0.35	0.53	0.866	0.024
$< \eta >_{MWL}$	0.25	0.41	0.797	0.019
$< \eta >_{LWL}$	0.20	0.43	0.648	0.018

NHESSD
3, 3077–3117, 2015

Table 3. Return values for R_{high} corresponding to 5, 10, 50, and 100 years return period with the 95 % confidence bounds values.

Return period	R_{high}	
	reconstructed	parameterized
(yr)	(m)	(m)
5	1.723	1.796
10	1.775	1.844
50	1.856	1.905
100	1.88	1.92

NHESSD
3, 3077–3117, 2015

Table 4. Return values for R_{low} corresponding to 5, 10, 50, and 100 years return period with the 95 % confidence bounds values.

Return period	R_{low}	
	reconstructed	parameterized
(yr)	(m)	(m)
5	0.7962	0.7861
10	0.8265	0.8142
50	0.8711	0.8543
100	0.8835	0.8651

NHESSD
3, 3077–3117, 2015

Table 5. Storm impact regimes corresponding to the 5, 10, 50, and 100 years return value of R_{high} and R_{low}, considering a value of D_{high} and D_{low} of 2.27 and 0.8 m respectively; and a typical value of storm surge (≈ 0.5 m).

Return period (yr)	R_{high} (m)	R_{low} (m)	Storm impact regime	
			no storm surge	w/storm surge
5	1.723	0.7962	collision	collision
10	1.775	0.8265	collision	overwash
50	1.856	0.8711	collision	overwash
100	1.88	0.8835	collision	overwash

NHESSD
3, 3077–3117, 2015

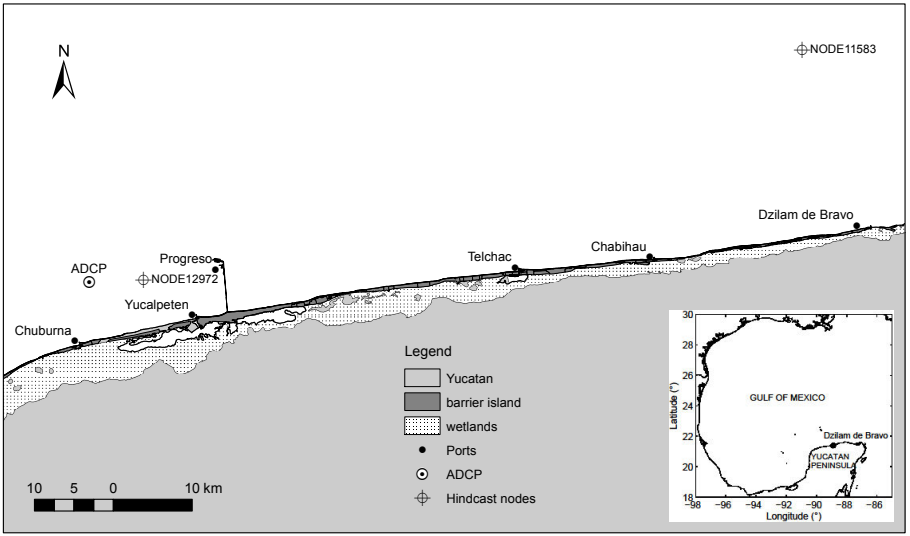

Figure 1. Location map indicating the study site (Dzilam de Bravo) at the barrier island backed by the wetlands and the mainland of Yucatan Peninsula, the position of the hindcast nodes used for the simulations, and the ADCP location in between of Chuburna and Yucalpeten ports.

NHESSD
3, 3077–3117, 2015

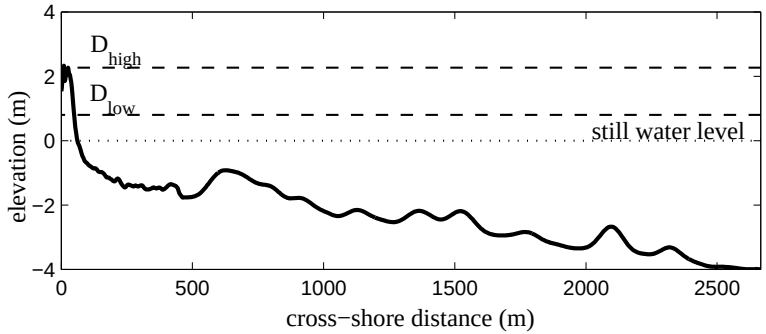

Figure 2. Beach profile indicating the dune crest (D_{high} = 2.27 m) and dune base (D_{low} = 0.8 m) elevations with respect to still water level.

NHESSD
3, 3077–3117, 2015

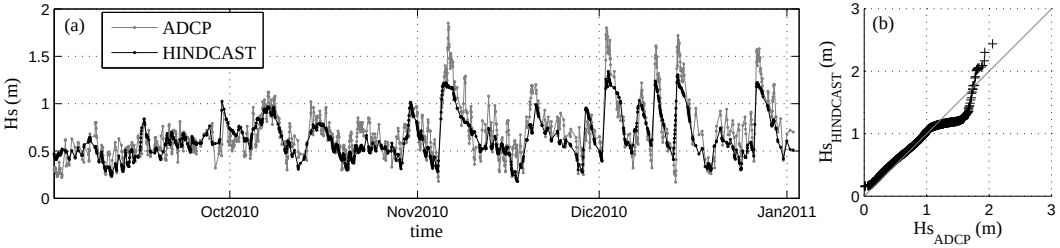

Figure 3. (a) Time series section of observed and hindcast significant wave height and **(b)** QQ-plot showing the comparison between ADCP wave data and modeled Hindcast data at a location close to the study area. Solid line in **(b)** indicates perfect correlation.

NHESSD
3, 3077–3117, 2015

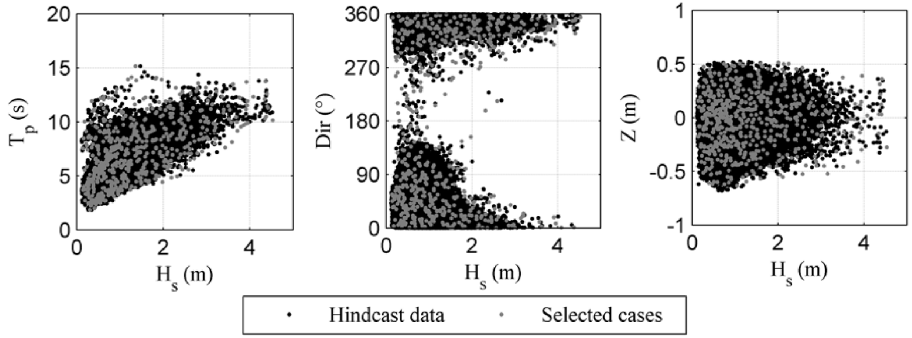

Figure 4. Significant wave height (H_s) against wave period (T_p) and mean direction corresponding to the 30 year wave hindcast data, and astronomical tide (Z), showing the distribution of the selected cases using the MDA algorithm for M = 600.

NHESSD
3, 3077–3117, 2015

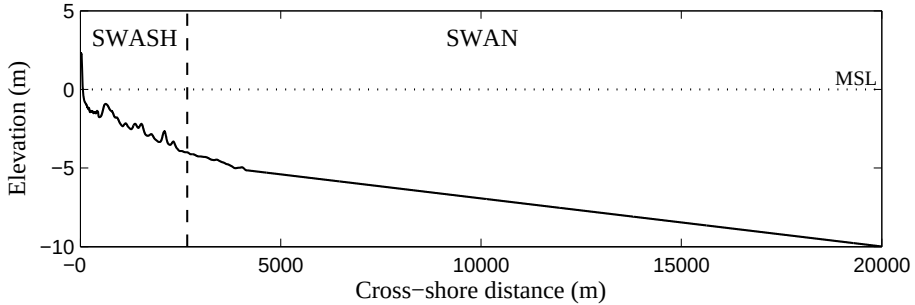

Figure 5. Beach profile at Dzilam showing the section corresponding to simulations performed by the SWAN model (10–4 m depth) and the section for SWASH simulations (4 m depth to shore). Dotted line represents the mean sea level.

NHESSD
3, 3077–3117, 2015

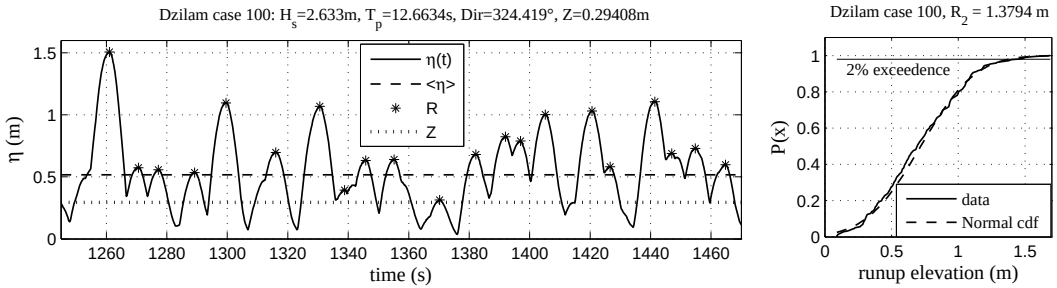

Figure 6. Section of water level elevation time series relative to mean sea level ($\eta(t)$) extracted from the wet–dry boundary of SWASH simulations for every sea state propagated to shore, indicating tide Z, runup maxima, R, and setup at the shoreline $<\eta>$ (left panel). The 2 % exceedence value was extracted from the cumulative PDF of the R values (right panel).

NHESSD
3, 3077–3117, 2015

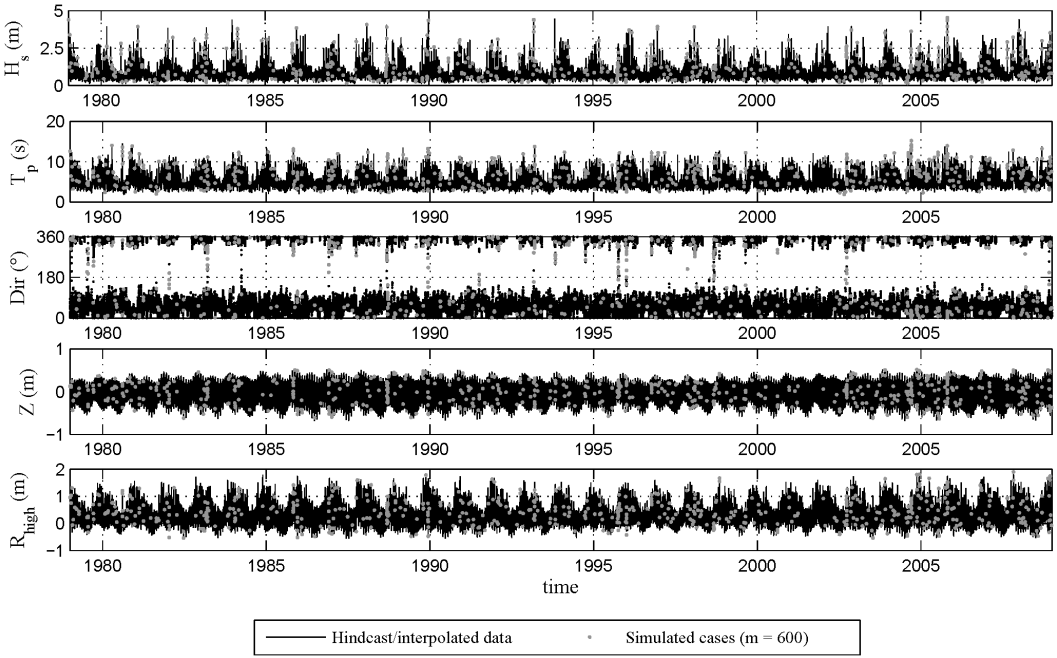

Figure 7. Time series of the wave hindcast data (H_s, T_p, θ), sea level (Z), and interpolated runup value ($R_{high} = R_{2\%} + Z$), indicating the selected/simulated cases.

NHESSD
3, 3077–3117, 2015

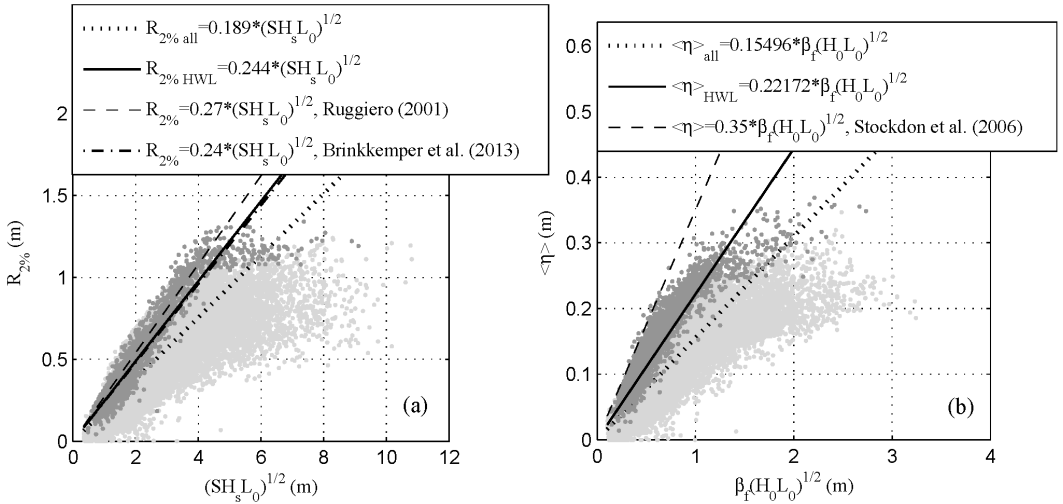

Figure 8. Linear fit to **(a)** $R_{2\%}$ values associated to high water level ($Z \geq Z_{5\%} = 0.32$ m, darker grey dots), and comparison to Ruggiero et al. (2001) and Brinkkemper et al. (2013) parametrizations, and **(b)** setup values (all and HWL) compared to Stockdon et al. (2006) parameterization. The dotted line corresponds to the linear fit performed to the entire set of data.

NHESSD
3, 3077–3117, 2015

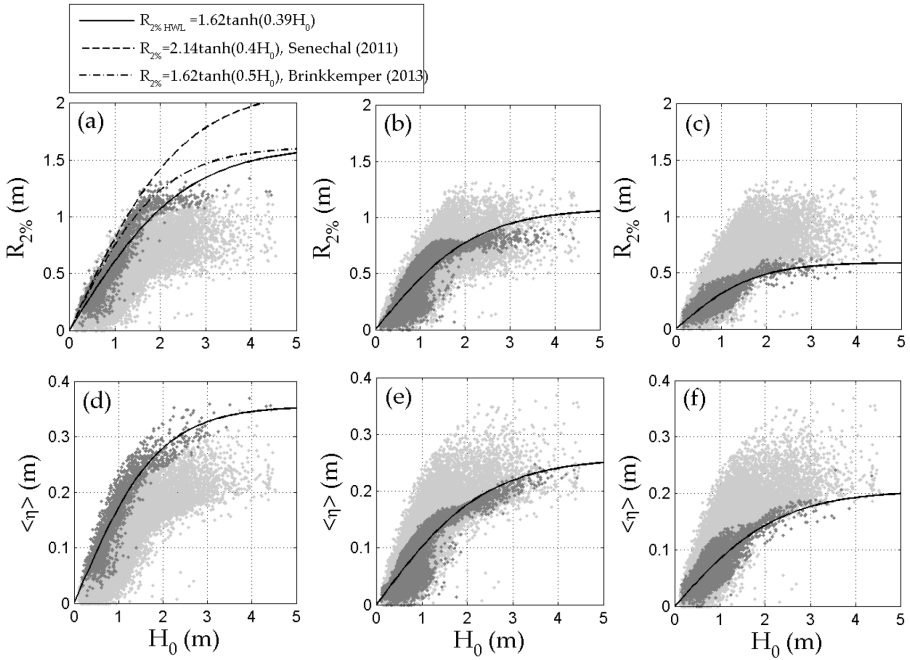

Figure 9. Hyperbolic tangent fit of $R_{2\%}$ and $< \eta >$ values associated to **(a, d)** high water level ($Z \geq Z_{5\%} = 0.32$ m), **(b, e)** mean water level ($0.05 \geq Z \geq -0.05$ m), and **(c, f)** low water level ($Z \leq Z_{5\%} = -0.32$ m), represented by the darker grey dots. Comparison to Senechal et al. (2011) and Brinkkemper et al. (2013) expressions in **(a)** for $R_{2\%}$ values associated to high water level.

NHESSD
3, 3077–3117, 2015

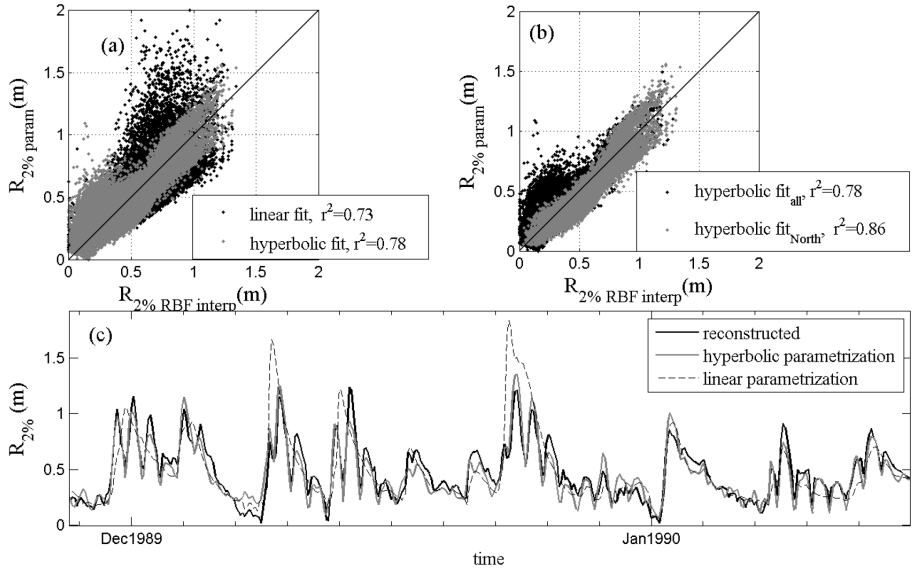

Figure 10. Reconstructed $R_{2\%}$ values obtained from the RBF interpolation correlated against $R_{2\%}$ values obtained from **(a)** linear vs. hyperbolic tangent fits, and **(b)** hyperbolic tangent fit to all $R_{2\%}$ values vs. the ones corresponding to waves approaching from the North ($337.5 \leq \theta \leq 22.5$), **(c)** comparison of a timeseries section of reconstructed vs. parameterized $R_{2\%}$ values.

NHESSD
3, 3077–3117, 2015

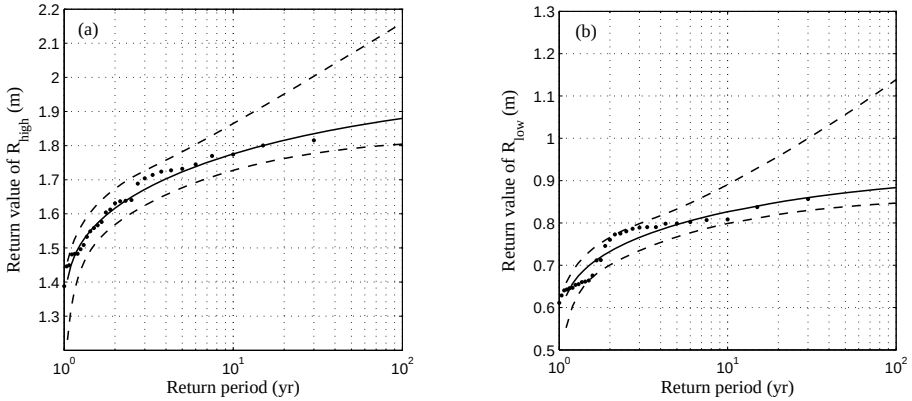

Figure 11. Return value extrapolation of **(a)** R_{high} and **(b)** R_{low} in the GEV model with the 95 % confidence bounds.

NHESSD
3, 3077–3117, 2015